

Reynolds number scaling of influence of boundary layers on the global behavior of laboratory quasi-Keplerian flows

E. M. Edlund and H. Ji

Princeton Plasma Physics Laboratory, Princeton, New Jersey 08543, USA

Abstract

We present measurements of quasi-Keplerian flows in a Taylor-Couette device that identify the boundary conditions required to generate near-ideal flows that exhibit self-similarity under scaling of the Reynolds number. These experiments are contrasted with alternate boundary configurations that result in flows that progressively deviate from ideal Couette rotation as the Reynolds number is increased. These behaviors are quantitatively explained in terms of the tendency to generate global Ekman circulation and the balance of angular momentum fluxes through the axial and radial boundary layers.

The idea that the global properties of an extended system may be mapped to the boundaries has found success in holographic theories in general relativistic systems [1, 2], and in magnetically confined plasmas [3, 4] where the global energy confinement is largely determined by the shear at the plasma boundary. In the studies reported here, we examine rotating flows in a Taylor-Couette apparatus and investigate the relationship between the forcing induced at the boundaries and the resulting global rotation in the bulk of the volume. Numerous recent experiments in Taylor-Couette devices have focused on astrophysically-relevant flows as a means for exploring the nature of angular momentum transport in accretion disks through incompressible hydrodynamic turbulence [5, 6, 7, 8], with extensions magnetohydrodynamics in electrically conducting fluids [9, 10, 11, 12]. Understanding the stability of the bulk flow in such experiments implies a requirement to understand the influence of the boundaries. Quasi-Keplerian flows, that is, rotation satisfying $0 < q < 2$ where $q = -d \ln \Omega / d \ln r$, are linearly stable but it is unknown whether there exists a nonlinear transition to turbulence. Experiments seem to indicate not [5, 6, 7].

Prior laboratory studies of astrophysically-relevant flows have established the use of independent rings on the axial boundaries as a reliable method to reduce the Ekman circulation that is driven by differences between the bulk flow and boundaries, resulting in azimuthal rotation profiles very nearly matching that of ideal Couette rotation [5, 7, 13, 14]. These studies have identified the important role of boundary layers, though the phenomenology of such flows has not been quantitatively explained. The experiments reported here provide an insight into the competing roles of axial (Ekman) and radial (Stewartson) boundary layers, such that self-similarity of the mean profiles can be maintained, as the Reynolds number is scaled, only for a narrow window range of boundary conditions. There is a growing awareness of the important role of the axial boundaries [15], but until now there has not existed a comprehensive model for the balance of radial and axial fluxes. How these systems trend as the speeds are increased is revealing of whether they are dominated by boundary interactions or internal dynamics, a distinction with important consequences for the applicability of such experiments to interpretation of astrophysical systems.

The flows in Taylor-Couette experiments transition from the bulk flow to the axial boundary speeds over Ekman boundary layers whose thickness scales like $\delta_E \sim r \text{Re}_b^{-1/4}$, and in the ideal model of radial boundaries, over Stewartson boundary layers that scale like $\delta_S \sim r \text{Re}_b^{-1/4}$, where $\text{Re}_b = r^2 \Omega_b / \nu$ is a local Reynolds number particular to the boundary location r with boundary speed Ω_b [16, 17, 18]. The fluxes of angular momentum across these boundary layers, being inversely proportional to the boundary layer thickness, do not scale proportionally, and hence we anticipate violations of self-similarity in the global properties as the Reynolds number is scaled. This is indeed what is observed in experiment when measures are not taken to mitigate the influence of the axial boundaries, and the goal of this work is to show that the global properties of Taylor-Couette systems can largely be interpreted as a response to the flux of angular momentum across the radial and axial boundaries.

We begin by examining experiments conducted in the HTX device where three different boundary configurations are illustrated in Fig. 1: **Split** configurations at multiples of 350-350-50 RPM, **Optimized** configurations at multiples of 350-185-50 RPM, and **Ekman** configurations at multiples of 350-50-50 RPM, where the speeds are reported as Ω_1 - Ω_3 - Ω_2 . The apparatus used in these studies has an inner cylinder radius of $r_1 = 6.9$ cm, an outer cylinder radius of $r_2 = 20.3$ cm, and an axial length of $L = 39.8$ cm. Measurements of the fluid velocity are conducted with a laser Doppler velocimetry diagnostic. The angular velocities of the inner cylinder, outer cylinder and rings are identified by Ω_1 , Ω_2 and Ω_3 , respectively. For these studies we define the shear Reynolds number as $\text{Re}_s = r_g^2 \Delta \Omega / \nu$, where $r_g = (r_1 r_2)^{1/2}$ is the geometric-mean radius, $\Delta \Omega = \Omega_1 - \Omega_2$, and ν is the kinematic viscosity. Most strikingly, the **Optimized** configurations show negligible departure

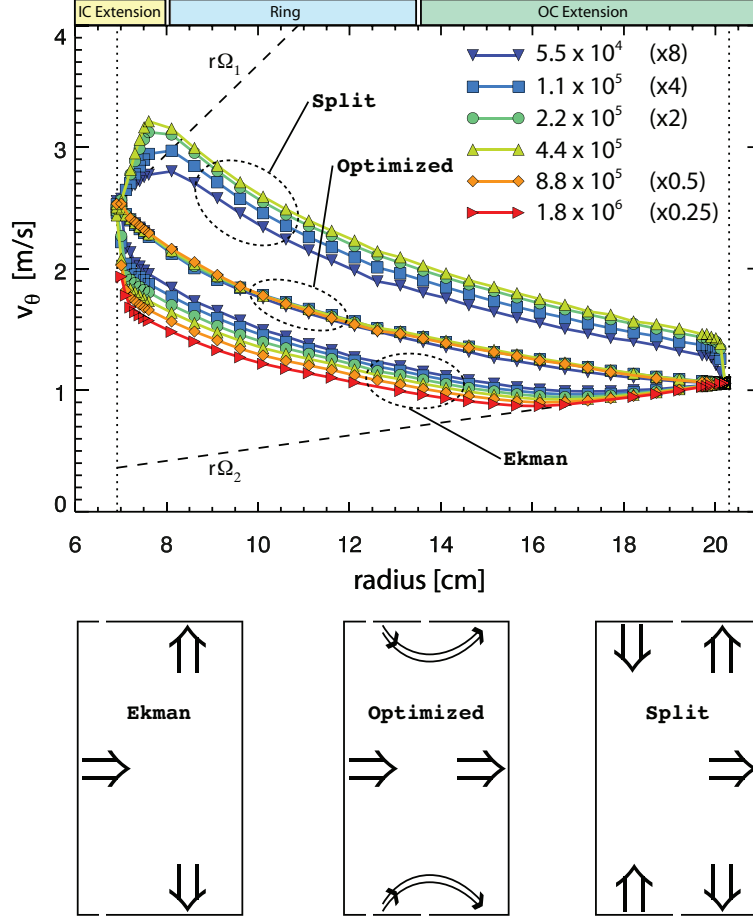


Figure 1: (color online) Measurements of the azimuthal velocity profiles at the Re_s indicated in the legend, with the scaling factor in parentheses. The speeds are scaled by powers of 2 relative to the reference case of $\Omega_1 = 350$ RPM and $\Omega_2 = 50$ RPM ($Re_s = 4.4 \times 10^5$). Three different configurations are studied: the “classical” or **Ekman** configuration with $\Omega_3 = \Omega_2$ (lower group), an **Optimized** configuration with Ω_3 equal to multiples of 185 RPM (middle group) and the **Split** configuration where $\Omega_3 = \Omega_1$ (top group). The radial extent of the axial boundary components is indicated at the top. The illustrations at the bottom indicate the dominant fluxes of angular momentum across the boundaries inferred by these studies.

from the ideal Couette profile over a wide range of Re_s . However, the **Ekman** and **Split** cases show progressive departure from ideal Couette rotation as Re_s is increased. The subsequent discussions identify the conditions required to achieve nearly-ideal flows in the **Optimized** configuration, and then develop a model to explain the role of boundary layers in determining the observed deviations from ideal Couette in the **Ekman** and **Split** configurations.

The framework for interpretation of these observations is that in steady-state the net flux of angular momentum into the flow must sum to zero, that is, $\Phi_1 + \Phi_2 + 2\Phi_z = 0$ where Φ_1 and Φ_2 are the fluxes across the inner and outer cylinders, respectively, and Φ_z is the axial flux across each axial boundary. In the presence of purely radial, viscous transport, a constant flux of angular momentum will be established, with a magnitude equal to

$$\Phi_C = 4\pi\rho\nu \frac{L r_g^4}{r_2^2 - r_1^2} \Delta\Omega, \quad (1)$$

from which we find the ideal Couette solutions for the rotation profile $\Omega_C(r) = \Omega_A + \Omega_B(r_g/r)^2$, where $\Omega_A = (r_2^2\Omega_2 - r_1^2\Omega_1)/(r_2^2 - r_1^2)$, $\Omega_B = r_g^2(\Omega_1 - \Omega_2)/(r_2^2 - r_1^2)$. Under these conditions we have $\Phi_2 = -\Phi_1$, implying that the ideal flow has $\Phi_z = 0$ everywhere. As will be shown, we find that nearly-ideal Couette flows may be achieved in practice by satisfying the weaker constraint that the surface integral of Φ_z vanish.

The axial flux of angular momentum across the axial boundaries occurs over Ekman boundary layers whose absolute thickness is in the sub-mm range at the experimental Reynolds numbers examined here. In lieu of detailed measurements of the Ekman boundary-layer structure, we make the simplifying assumptions that $d\Omega/dz \approx \Delta\Omega_E/\delta_E$, where $\Delta\Omega_E = \Omega_b - \Omega_f$ is the difference of the boundary angular velocity and fluid angular velocity just inside the boundary layer, and that $\delta_E = \alpha_E \sqrt{\nu/\Omega_b}$ represents the thickness of an Ekman boundary layer with an unknown numerical constant α_E . Taking the reference flow for which we aim to achieve to be the ideal Couette flow, we inquire under what conditions the total axial flux (Φ_z) vanishes, where

$$\Phi_z = -\frac{2\pi\rho\nu}{\alpha_E} \int_{r_1}^{r_2} r^3 (\Omega_b - \Omega_C) \left(\frac{\Omega_b}{\nu}\right)^{1/2} dr. \quad (2)$$

That the radial flux of angular momentum under ideal Couette rotation (Eq. 1) scales like Re_s , whereas Φ_z scales like $\text{Re}_s^{3/2}$ means that unless steps are taken to minimize the axial flux by forcing the integral in Eq. 2 to zero, the axial boundaries will eventually overwhelm the radial flux and force the flow to depart from ideal rotation, regardless of aspect ratio. To examine the role of the axial boundaries in dictating optimal performance, we compare the configuration from the experiments of Fig. 1, which we term the **HTX** configuration, with a **wide-ring** configuration, and scan Ω_3 as presented in Fig. 2. The **HTX** configuration produces an exceptional match to the ideal Couette profile for a narrow range of ring speeds centered about 185 RPM, with very low fluctuation levels spanning the entire gap [7]. In contrast, the **wide-ring** configuration exhibits only relatively poor performance for all ring speeds.

Calculations of Φ_z for the **HTX** and **wide-ring** configurations, as a function of the ring speed, are presented as the red curves in panels (c) and (d) of Fig. 2. For the **HTX** configuration we find that the range of conditions defined by low fluctuation levels and small departure from ideal Couette rotation is very nearly coincident with the zero of Φ_z . However, the **wide-ring** case also has a zero in Φ_z , yet its flows never resemble ideal Couette, clearly indicating that the vanishing of Φ_z is not a sufficient condition for achieving optimal performance.

The role of the axial boundaries has previously been interpreted from the perspective of pressure balance between the Couette flow and boundary flow (of the fluid that is nearly tied to the solid body rotation of the axial boundaries), with pressure balance as a condition dictating optimum performance [19, 20]. The tendency of these systems to drive secondary flows was shown to be consistent with whether the pressure produced by the Couette rotation is larger than (Ekman circulation) or smaller than (anti-Ekman circulation) the pressure in the boundary layers. Following the intuition motivated by these simulations, we define a function Δp that characterizes the radial average of the pressure differences between ideal Couette rotation and boundary rotation,

$$\Delta p = \frac{1}{\Delta r} \int_{r_1}^{r_2} \int_{r_1}^r \rho r' (\Omega_C^2 - \Omega_b^2) dr' dr, \quad (3)$$

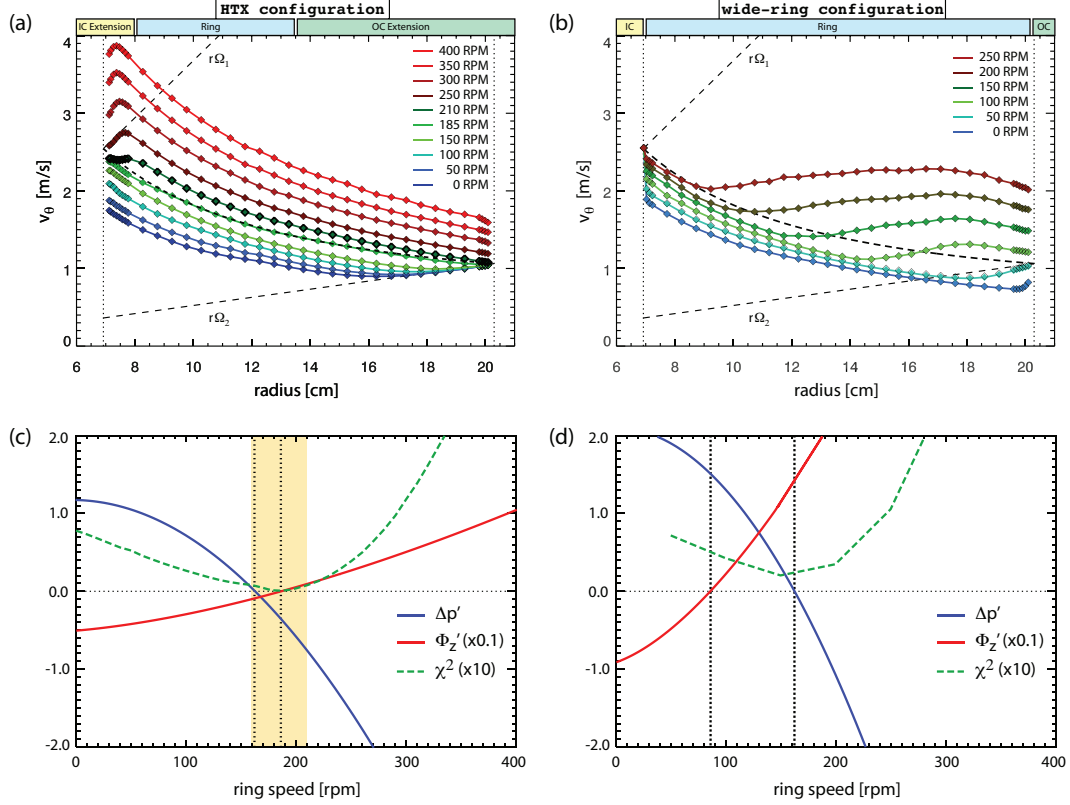


Figure 2: (color online) (a)-(b) show measured radial profiles of the azimuthal velocity, as a function of ring speed for the HTX and **wide-ring** geometries, respectively. Plots (c)-(d) show the calculated normalized pressure differential from Eq. 3 (blue), normalized axial flux of angular momentum according to Eq. 2 (red), and the experimental χ^2 (dashed green). Δp is normalized by the kinetic energy density, assuming ideal Couette flow, and Φ_z is normalized by the ideal Couette flux of angular momentum, Φ_C of Eq. 1. The vertical dotted lines indicate the zeros of Δp and Φ_z and the beige band in panel (a) indicate the range of ring speeds for which negligible fluctuations were observed in the studies of ref. [7].

Calculations of Δp are presented as the blue curve in panels (c) and (d) of Fig. 2, showing that the zero of Δp is widely separated from the zero of Φ_z for the case of the **wide-ring** configuration, suggesting that no circumstance exists where pressure balance and zero net flux can be simultaneously satisfied. In contrast, the HTX configuration has zeros very nearly coincident, and within the range of small fluctuations identified in Ref. [7]. We note that similar experiments have been conducted with a ring configuration matching that of a different experiment [14], modified from the HTX configuration by extending the inner boundary of the ring to r_1 , where it was observed that optimum performance occurs at 200 RPM, in good agreement with an increase in both zeros of Φ_z and Δp by nearly that same amount.

While the occurrence of zeros in both Φ_z and Δp may largely explain the conditions under which ideal performance may be achieved, they do not reveal how these systems should behave under non-optimized conditions. To develop a general understanding of the fluid response to forcing by the boundaries we must include the fluxes across both axial and radial boundary layers. As there does not exist a complete theory of Stewartson boundary layers under the conditions of large Reynolds number, large shear and quasi-Keplerian rotation, we cannot rely on results derived from a linear

analysis of perturbative differences in rotational speeds, especially for these experiments where the Stewartson boundary layers are known to be turbulent [7]. Instead, we assume a generalized scaling of the Stewartson boundary layer of the form $\delta_S = \alpha_S r \text{Re}_b^\beta$, taking the dependence on Reynolds number (β) as a free-parameter to be determined from the observed scalings in Fig. 2. While the numerical factors α_E and α_S enter through the definitions of the boundary layer thicknesses, we must interpret their meaning as a measure of the effectiveness of angular momentum flux across the respective boundary layer, with smaller values indicating larger effective fluxes. With this in mind, it may be expected that $\alpha_S \ll \alpha_E$ given the vigor of the centrifugal instability in the radial boundary layers.

A general analysis is complicated by the presence of three terms in the boundary flux balance. However, we exploit a fortunate circumstance to simplify the problem. We observe that the v_θ for the lower group of profiles (**Ekman** configuration) presented in Fig. 2 are decently modeled as an ideal Couette profile that is offset by a constant Δv , up to a region near the outer cylinder where the flow transitions to solid body rotation at Ω_2 , implying that $\Phi_2 \approx 0$. With a Stewartson layer present at the inner cylinder, the appropriate form for Φ_1 is

$$\Phi_1 = -2\pi \frac{c_1}{\alpha_S} \rho \nu L r_1 \text{Re}_s^\beta \Delta v, \quad (4)$$

where $c_1 = (r_1 \Omega_1 / r_2 \Delta \Omega)^\beta$ is a result of converting from a boundary layer depending on Re_b to Re_s . To calculate Φ_z for the **Ekman** configuration with negative values of Δv , we approximate the flow as a piecewise function of the form

$$v_\theta(r) = \begin{cases} r\Omega_c + \Delta v & \text{for } r_1 < r < r_t \\ r\Omega_2 & \text{for } r_t < r < r_2 \end{cases} \quad (5)$$

where r_t is the transition radius at which the shifted ideal Couette profile is continuous with the outer region under solid body rotation at Ω_2 . Using the forms for the axial and radial fluxes given in 2 and 4 we solve global balance of angular momentum $\Phi_1 + 2\Phi_z = 0$ for the dimensionless $\Delta v'_{\text{neg}} = \Delta v / r_g \Delta \Omega$, as a function of Re_s . Noting that Δv occurs in both Φ_1 and Φ_z , our solution has three terms and is represented by the following form

$$\Delta v'_{\text{neg}} = \frac{f_1(x_t)}{\alpha c_1 \frac{L}{2r_2} \text{Re}_s^{\beta-0.5} + f_2(x_t)}, \quad (6)$$

where $\alpha = \alpha_E / \alpha_S$ and the dimensionless functions $f_1(x_t)$ and $f_2(x_t)$, derived from the integral in Eq. 2, are defined in the supplement for $x_1 = r_1 / r_g$, $x_2 = r_2 / r_g$, $x_t = r_t / r_g$, $\Delta \omega = (\Omega_b - \Omega_C) / \Delta \Omega$ and $\omega_b = \Omega_b / \Delta \Omega$. Equation 6 is a transcendental expression in Δv since the limits of the integrals in f_1 and f_2 are functions of r_t which itself depends on Δv . Equation 6 has only two free parameters: the ratio of the coefficients of the Ekman and Stewartson boundary layers (α_E / α_S) and the scaling coefficient of the Stewartson boundary layer thickness (β). Comparison of Eq. 6 with experimental measurements of Δv is presented in Fig. 3, where values of $\beta \approx 0.1$ and $\alpha_E / \alpha_S \approx 55$ provide the best fit to the experimental measurements. Recalling that α_S^{-1} is a measure of effectiveness of angular momentum flux through a Stewartson boundary layer, $\alpha_E / \alpha_S \approx 55$ points to a radial flux of angular momentum through turbulent Stewartson boundary layers that is far more effective than that through the Ekman layers, confirming the earlier suspicion that the turbulent Stewartson layers have very strong relative transport of angular momentum.

This analysis can be extended to the case of the **Split** configuration with positive Δv with modifications to account for the slightly more complex response and different boundary conditions. The most important feature of the positive Δv cases is that there is a nearly linear decrease in

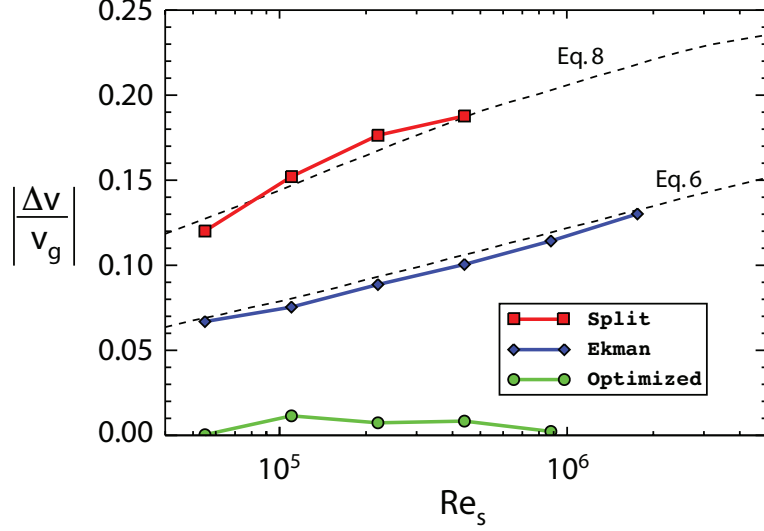


Figure 3: (color online) Scaling of the velocity differential Δv for the three groups of boundary conditions from Fig. 2 identified by the reference case with $\Omega_1 = 350$ RPM and $\Omega_2 = 50$ RPM. The dashed lines in the figure are the solutions to Eqs. 6 and 8 with $\beta = 0.10$ and $\alpha_E/\alpha_S = 55$. The 350 – 50 – 50 cases have negative values of Δv , and are presented here as the absolute value for ease of comparison. The results of the optimized cases (green) are shown only for reference as the theory does not apply to them since $\Phi_z \approx 0$.

Δv across the gap, with Δv near r_2 about 60 percent of the peak value, seemingly independent of Reynolds number. While in these cases there is a nonzero gradient of Ω near the inner cylinder, and hence a finite radial flux of angular momentum, these gradients are still many times smaller in magnitude than those found near the outer cylinder, and being laminar [7], have negligible impact on the overall transport balance, allowing us to approximate the solution by taking $\Phi_1 \approx 0$. Under these conditions, the radial flux of angular momentum near the outer cylinder is

$$\Phi_2 = 2\pi \frac{c_2}{\alpha_S} \rho \nu L r_2 \text{Re}_s^\beta (0.6\Delta v), \quad (7)$$

where $c_2 = (r_2\Omega_2/r_1\Delta\Omega)^\beta$ and f_3 and f_4 are integrals similar to those of Eq. 6, but modified for the specifics of the **Split** configuration, whose forms are provided in the supplement. The solution for positive, normalized Δv is

$$\Delta v'_{pos} = \frac{f_3(x_t)}{0.6c_2 \frac{L}{2r_1} \alpha \text{Re}_s^{\beta-0.5} + f_4(x_t)}, \quad (8)$$

Equation 8 is compared against the measured Δv in Fig. 3, and found also to be in good agreement when using the same values the α_E/α_S and β derived from the analysis of Eq. 6.

While we cannot offer a precise theoretical explanation for why β should take a value close to 0.1, we recall that α_E and α_S measure the effectiveness of the angular momentum fluxes, and hence the net transport will be confounded by the presence of a turbulent viscosity. Building on the work established in [7] where a transition to turbulent boundary layers was observed to be consistent with the Taylor model of low Reynolds number centrifugal instability, it is likely that the vigorous turbulence in these cases should be represented by a turbulent viscosity, ν_{turb} , that itself increases with Reynolds number. Thus, the influence of ν_{turb} will give rise to an apparently weaker scaling

with Reynolds number (compared to the case of a simple laminar viscosity) as the larger viscosity counteracts to some extent the decrease of the Stewartson boundary layer thickness. Additional dedicated experiments are needed to resolve the separate dependence of ν_{turb} from the scaling of the boundary layer thickness itself.

While this analysis provides a succinct and intuitive method for interpreting global behavior, it raises additional questions that cannot yet be answered. Foremost among these is what enables the profiles to violate the implications of the Taylor-Proudman theorem, especially considering that the local flux of angular momentum may be quite large, and it is only on summing over the axial boundaries that zero net flux is realized. Given that these modified Taylor-Couette devices exhibit nearly uniform axial structure [14], it seems that in order to maintain ideal Couette profiles that are in conflict with the axial boundaries, the angular momentum fluxes through the Ekman boundary layers must be redistributed rather locally, likely by small Ekman cells that do not extend far into the bulk of the fluid. As was shown in an earlier experiment, the free-shear layer that develops at the interface between the differentially rotating rings on the axial boundaries is expected to be unstable and may help to redistribute angular momentum locally [12].

We conclude with an outlook to future physical and numerical experiments. The ratio of Φ_z and Φ_C explored earlier can be recast as a constraint on the aspect ratio $L/\Delta r$ as a function of the Reynolds number. The relative contribution of Φ_z can be made arbitrarily small by increasing the length of the system, so that to make $\Phi_z/\Phi_C \approx 10^{-2}$ for an **Ekman** configuration, for example, one would need an aspect ratio of order 10^2 at a Reynolds number of order 10^6 . Despite the desire to simplify the mechanics of Taylor-Couette experiments, further analysis shows that the only way to achieve simultaneous zeros in Φ_z and Δp is by using a device with at least one independent ring.

The picture of balanced radial and axial fluxes that emerges from the Reynolds number scaling presented here provides the conceptual framework for predictive capability of global flow behavior. Among the **Optimized** configurations there appears to be little variation as the Reynolds number is scaled, consistent with the vanishing of the pressure differential and the axial flux of angular momentum. Non-optimized boundary configurations, like the **Split** and **Ekman** configurations, show progressively larger departure from the ideal Couette flow as the Reynolds number is increased. The same numerical values of α_E/α_S and β apply equally well to cases with positive and negative Δv , supporting a unified model of turbulent transport of angular momentum through boundary layers. A problem for future experiments, both physical and numerical, will be to explore in greater detail how the very large, local fluxes of angular momentum are redistributed near the axial boundaries with only minor effect on the bulk flow in the **Optimized** configurations. A good test for numerical experiments will be to accurately model the global behavior of Taylor-Couette experiments by including models of the boundary layers. We believe that the boundary layer scalings presented here may enable simulations to bootstrap to larger effective Reynolds numbers by using specified boundary flux models, thus bypassing the need for very fine grids to resolve the boundary layer structure directly.

References

- [1] A. Adams, P. M. Chesler, and H. Liu. Holographic Turbulence. *Phys. Rev. Lett.*, 112:151602, 2014.
- [2] F. Carrasco, L. Lehner, R. C. Myers, O. Reula, and A. Singh. Turbulent flows for relativistic conformal fluids in 2+1 dimensions. *Phys. Rev. D*, 86:126006, 2012.
- [3] J. E. Rice, J. W. Hughes, P. H. Diamond, Y. Kosuga, Y. A. Podpaly, M. L. Reinke, M. J. Greenwald, Ö. D. Gürçan, T. S. Hahm, A. E. Hubbard, E. S. Marmor, C. J. McDevitt, and D. G. Whyte. Edge temperature gradient as intrinsic rotation drive in alcator *c*-mod tokamak plasmas. *Phys. Rev. Lett.*, 106:215001, 2011.
- [4] O. D. Gurcan, P. H. Diamond, C. J. McDevitt, and T. S. Hahm. A simple model of intrinsic rotation in high confinement regime tokamak plasmas. *Phys. Plasmas*, 17:032509, 2010.
- [5] H. Ji, M. Burin, E. Scharfman, and J. Goodman. Hydrodynamic turbulence cannot transport angular momentum effectively in astrophysical disks. *Nature*, 444:343, 2006.
- [6] E. Scharfman, H. Ji, M. Burin, and J. Goodman. Stability of quasi-Keplerian shear flow in a laboratory experiment. *Astron. Astrophys.*, 543:A94, 2012.
- [7] E. M. Edlund and H. Ji. Nonlinear stability of laboratory quasi-keplerian flows. *Phys. Rev. E*, 89:021004, 2014.
- [8] M. S. Paoletti and D. P. Lathrop. Angular momentum transport in turbulent flow between independently rotating cylinders. *Phys. Rev. Lett.*, 106:024501, 2011.
- [9] F. Stefani, T. Gundrum, G. Gerbeth, G. Rüdiger, M. Schultz, J. Szklarski, and R. Hollerbach. Experimental evidence for magnetorotational instability in a taylor-couette flow under the influence of a helical magnetic field. *Phys. Rev. Lett.*, 97:184502, 2006.
- [10] D. R. Sisan, N. Mujica, W. A. Tilletson, Y. Huang, W. Dorland, A. B. Hassam, T. M. Antonsen, and D. P. Lathrop. Experimental observation and characterization of the magnetorotational instability. *Phys. Rev. Lett.*, 93:114502, 2004.
- [11] A. H. Roach, E. J. Spence, C. Gissinger, E. M. Edlund, P. Sloboda, J. Goodman, and H. Ji. Observation of a Free-Shercliff-Layer Instability in Cylindrical Geometry. *Phys. Rev. Lett.*, 108:154502, 2012.
- [12] E. J. Spence, A. H. Roach, E. M. Edlund, P. Sloboda, and H. Ji. Free magnetohydrodynamic shear layers in the presence of rotation and magnetic field. *Phys. Plasmas*, 19:056502, 2012.
- [13] M. Burin, H. Ji, E. Scharfman, R. Cutler, P. Heitzenroeder, W. Liu, L. Morris, and S. Raftopolous. Reduction of Ekman circulation within Taylor-Couette flow. *Experiments in Fluids*, 40:962, 2006.
- [14] E. Scharfman, H. Ji, and M. Burin. Development of a Couette-Taylor flow device with active minimization of secondary circulation. *Rev. Sci. Instrum.*, 80:024501, 2009.
- [15] F. Nordsiek, S. G. Huisman, R. C. A. van der Veen, C. Sun, D. Lohse, and D. P. Lathrop. Azimuthal velocity profiles in Rayleigh-stable Taylor-Couette flow and implied axial angular momentum transport. *arXiv*., 1408.1059:1, 2014.

- [16] D. A. Bennetts and L. M. Hocking. On nonlinear Ekman and Stewartson layers in a rotating fluid. *Proc. R. Soc. A.*, 333:469, 1973.
- [17] D. J. Baker. Shear layers in a rotating fluid. *J. Fluid Mech.*, 29:165, 1967.
- [18] K. Stewartson. On almost rigid rotations. *J. Fluid Mech.*, 3:17, 1957.
- [19] A. V. Obabko, F. Cattaneo, and P. F. Fischer. The influence of horizontal boundaries on Ekman circulation and angular momentum transport in a cylindrical annulus. *Phys. Scr.*, T132:014029, 2008.
- [20] O. Czarny, E. Serre, P. Bontoux, and R. Leuptow. Interaction between Ekman pumping and the centrifugal instability in Taylor-Couette flow. *Phys. Fluids*, 15:467, 2003.